Journal of Computational and Applied Mathematics 270 (2014) 78–87

Contents lists available at ScienceDirect

Journal of Computational and Applied Mathematics

journal homepage: www.elsevier.com/locate/cam

Three-dimensional simulation of a complete Vertical Axis Wind Turbine using overlapping grids

Michele Nini, Valentina Motta, Giampiero Bindolino, Alberto Guardone *

Department of Aerospace Science and Technology, Politecnico di Milano, Via La Masa, 34, 20156 Milano, Italy

ARTICLE INFO

Article history:
Received 2 October 2013

Keywords:
Vertical Axis Wind-Turbine
RANS
CFD
Overlapping grid
Finite volume scheme

ABSTRACT

Three-dimensional simulations of the aerodynamic field around a three-blade straight-axis Vertical Axis Wind Turbine (VAWT) are presented for two values of the Tip Speed Ratio λ (TSR), namely $\lambda = 1.52$ and $\lambda = 2.5$. Numerical simulations were carried out using the over-set grid solver ROSITA (ROtorcraft Software ITAly). The Reynolds-Averaged Navier–Stokes equations are completed by the Spalart–Allmaras turbulence model. A strong interaction between the blade and the blade wakes is evidenced. Dynamic stall is observed in the case $\lambda = 2.5$. The computed flow-field presents diverse three-dimensional effects, including the interaction between the blades and the tip vortices and the aerodynamic disturbances from the turbine shaft and the support arms. Three-dimensional effects are more relevant for $\lambda = 2.5$. The comparison to experimental data confirms the general features of the flow.

© 2014 Elsevier B.V. All rights reserved.

1. Introduction

Wind power represents one of the most relevant and promising renewable alternatives to fossil fuels. The most common devices used to extract wind energy are the horizontal axis wind turbines (HAWT). For medium to small power installation, vertical axis wind turbines (VAWT) can be preferred, due to insensitivity to the horizontal wind direction and low construction costs. Moreover, the lower noise emission makes vertical axis wind turbine more suitable for an urban environment. Unfortunately, the aerodynamic field around a VAWT is very complicated. Rotational motion and the peculiar geometry cause the occurrence of dynamic stall, the generation of tip vortices and the interaction between blades and shaft. As a result, the flow-field is fully tri-dimensional and it represents a challenging aerodynamic problem. A review of VAWT aerodynamics and technical peculiarities is presented in [1] for both the Savonius and the Darrieus VAWT types. In the present paper, the focus is on Darrieus-type turbines. In Refs. [2–4], the flow field around a straight-axis Darrieus-type VAWT is computed using a two-dimensional approximation, to investigate blade–wake interaction, the onset of dynamic stall and the optimal geometric configuration, including the airfoil shape, the optimal blade-to-axis distance and the number of blades. Reference experimental results for two-dimensional models are presented in [5–7], where the effects of the wind tunnel walls on the turbine aerodynamics are accounted for. Three-dimensional effects are studied in Refs. [8–10]. In [8], a single isolated blade is simulated for diverse airfoil geometry and blade solidity σ (airfoil chord to turbine diameter ratio). In [10], a comparison between three-dimensional simulations and experiments is presented for rotors with two and three blades, with a relatively large value of the solidity ($\sigma = 1, \sigma = 2/3$).

* Corresponding author.
E-mail address: alberto.guardone@polimi.it (A. Guardone).

http://dx.doi.org/10.1016/j.cam.2014.02.020
0377-0427/© 2014 Elsevier B.V. All rights reserved.

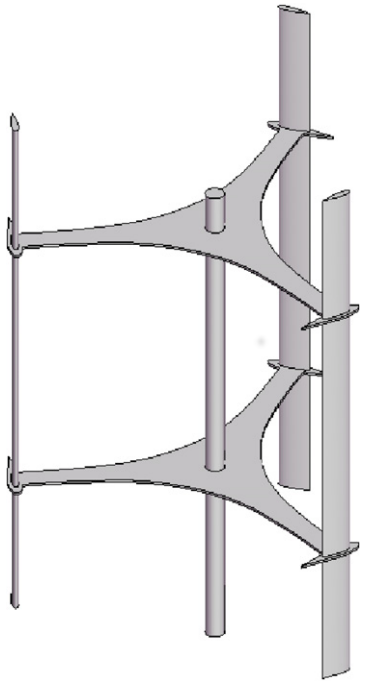

Fig. 1. Wind turbine geometry. All relevant parameters of the turbine geometry are listed in Table 1.

Table 1
VAWT geometric characteristics.

Blade length ($2H$)	1.457 m
Rotor diameter (D)	1.030 m
Solidity (Nc/D)	0.25
Blade airfoil	NACA0021
Chord (c)	0.086 m

In the present paper, three-dimensional simulations of a three-blade VAWT with $\sigma = 0.25$ are presented. The considered geometry is that proposed by Battisti and collaborators [11], for which experimental results are available and are used for comparison. The complete turbine configuration is modeled, including the shaft and the support structure. Differently from Ref. [9], here the support structure is composed by two flat radial elements (see Fig. 1) which are very relevant to the overall aerodynamic flow-field.

The paper is structured as follows: in Section 2, the VAWT model and the numerical method will be presented. In Section 3, results in symmetry and normal planes will be shown and compared with the available experimental data. Finally, in Section 4 concluding remarks are reported.

2. Model description

The turbine was designed and built by *Tozzi Nord Wind Turbine*, within a research project in collaboration with the University of Trento and Politecnico di Milano. The vertical axis wind turbine has three straight blades connected to the shaft by two support arms. The relevant VAWT parameters are reported in Table 1. The CAD model of the complete turbine is shown in Fig. 1.

2.1. Numerical method

Numerical simulations were performed using the finite-volume ROSITA solver developed at Politecnico di Milano for the solution of the Reynolds-Averaged Navier–Stokes (RANS) equations with the Spalart–Allmaras turbulence model [12].

The code is very suitable for the CFD study of moving and rotating bodies (e.g. rotors), due to the capability of treating a system of moving multi-block grids. A Chimera flux-interpolation technique allows to preserve a first/second order accuracy in space. The Chimera algorithm is based on the Chesshire and Henshaw method [13]; the basic idea is to interpolate the fluxes in overlapped regions, using as reference points those belonging to the finer grid. Loads over surfaces are finally

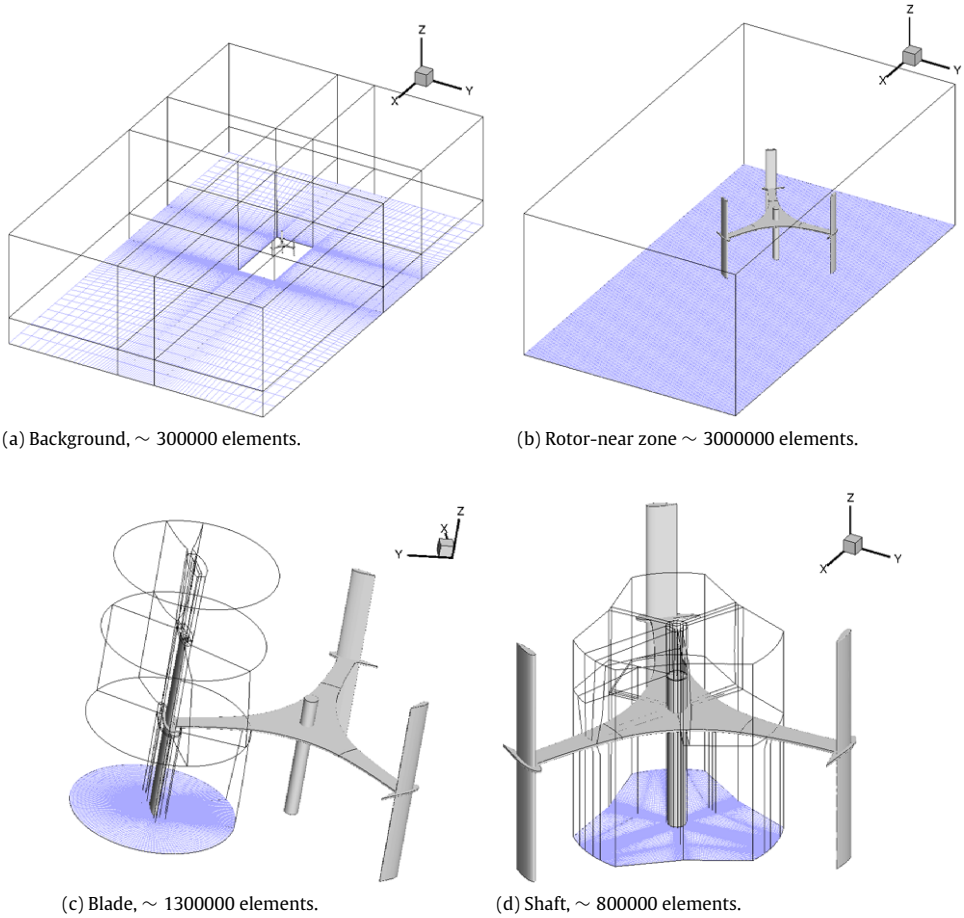

(a) Background, ∼ 300000 elements.

(b) Rotor-near zone ∼ 3000000 elements.

(c) Blade, ∼ 1300000 elements.

(d) Shaft, ∼ 800000 elements.

Fig. 2. Computational grids. Each grid is a multi-block structured grid of hexahedral elements, with the only exception of the Rotor-near zone grid which is a single-block grid.

calculated removing the overlapped cells from the coarser grids and triangulating the resulting gap between the grids, without adding new grid points.

The space discretization of RANS equations is obtained by means of a finite-volume cell centered implementation of Roe scheme, using a MUSCL extrapolation to attain second order accuracy in smooth-flow regions. The time derivative is approximated using an implicit dual time step cycle, combining a second order BDF formula with a backward Euler scheme for the pseudo-time iteration. Finally, the discretized system is solved with a preconditioned generalized conjugate gradient (GCG) method.

A detailed description of the Chimera technique and the flow solver implemented in ROSITA can be found in [14].

2.2. Computational domain

In the simulations, the flow symmetry with respect to the horizontal mid-span plane has been exploited to reduce the computational effort. As discussed in [5], this requires that the flow direction is normal to the turbine axis, namely, the turbine operates in a so-called horizontal flow.

The computational domain is composed by four different grids, see Fig. 2, with a total number of elements of about 8 millions. There are two background fixed grids: the former covers the whole far-field, whereas the latter is a finer mesh surrounding the rotor region. Furthermore, there is a cylindrical grid for each of the blades and one surrounding the shaft. These grids overlap at the center of the support arms. In the moving grids (c and d in Fig. 2), the spatial resolution is larger than that of background grids (a and b). In this way, thanks to the use of the Chimera technique, it is possible to obtain the desired grid spacing without increasing the computational effort. Moreover, grid nodes are clustered near to solid surfaces to increase boundary layer resolution and numerical stability. During the computation, the Chimera algorithm is used to account for the relative movement of the turbine with respect to the free stream. At every time step of the rotation, a new interpolation between the moving and the fixed grids is computed. In particular, a resolution of two degrees per time step was used here, therefore a total of 180 time steps are necessary.

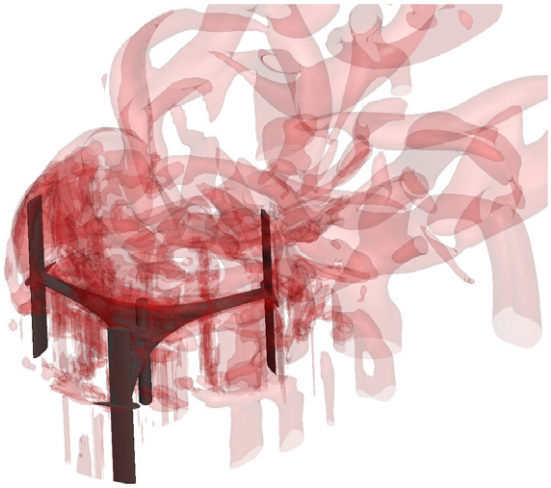

Fig. 3. Wake representation: iso-surfaces of $Q = \frac{1}{2}\left[|\mathbf{\Omega}|^2 - |\mathbf{S}|^2\right]$, in which $|\mathbf{\Omega}|^2$ and $|\mathbf{S}|^2$ represent the Euclidean norm of vorticity tensor and rate of strain tensor.

Table 2
Operating conditions.

λ ($\Omega R/U$)	2.5	1.52
Wind speed (U)	10.5 m/s	14.2 m/s
Rotational speed (Ω)	50.97 rad/s (486.72 rpm)	41.88 rad/s (400 rpm)

3. Numerical results

In this section numerical results are reported. An overview of the three-dimensional flow-field is given in Fig. 3, where the iso-surfaces of the quantity

$$Q = \frac{1}{2}\left[|\mathbf{\Omega}|^2 - |\mathbf{S}|^2\right], \tag{1}$$

are shown. In (1), $|\mathbf{\Omega}|^2$ and $|\mathbf{S}|^2$ are the Euclidean norm of the vorticity tensor and of the strain rate tensor, respectively. Q definition derived from the so-called Q-Criterion, one of the simplest and most popular criteria used to identify vortices [15].

The symmetry plane and a number of sections normal to the wind direction were considered. Simulations were carried out for two different operating conditions (Table 2). In Table 2, λ is the Tip Speed Ratio defined as:

$$\lambda = \frac{\Omega R}{U} \tag{2}$$

where U is the asymptotic wind speed and R the turbine radius. The two λ values herein investigated are $\lambda = 1.52$ and $\lambda = 2.5$.

Simulations have been performed over a cluster of 96 cores, with a clock speed of 2.66 GHz. Using a cycle of 50 pseudo-time steps for each real time step, an advancing speed of about 128 step per day has been obtained: considering the resolution of 2°, this leads to $\sim$ 256° of rotation per day. In the reference frame used in the following, X represents wind direction, Z the height and Y the span direction, the origin is located in symmetry plane in the center of VAWT.

3.1. Symmetry plane

In the symmetry plane ($Z = 0$) the X-velocity and (normal) Z-vorticity were analyzed. Figs. 4 and 5 show velocity field at five different times, corresponding to 30° of rotation, respectively for $\lambda = 2.5$ and $\lambda = 1.52$. The wake presents regions in which the velocity is close to zero, especially for $\lambda = 2.5$. In this configuration the wake is irregular and interference between the blades and the shaft in rotor area is observed. For the lower value of λ these phenomena are less important and the wake is quickly convected downstream, due to the larger free-stream velocity. It is interesting also noting the low speed region near the blade passing in the *south-west* position, which is the hallmark of dynamic stall. As observed by Fujisawa [7], dynamic stall angle depends on λ, in particular for lower λ, dynamic stall occurs at smaller angle of attack. Consequently, separated flow region is closer to the center of the rotor for $\lambda = 2.5$. In this case, a smaller value of the wind velocity, together with the occurrence of stronger interference, make dynamic stall for this configuration more significant. Fujisawa

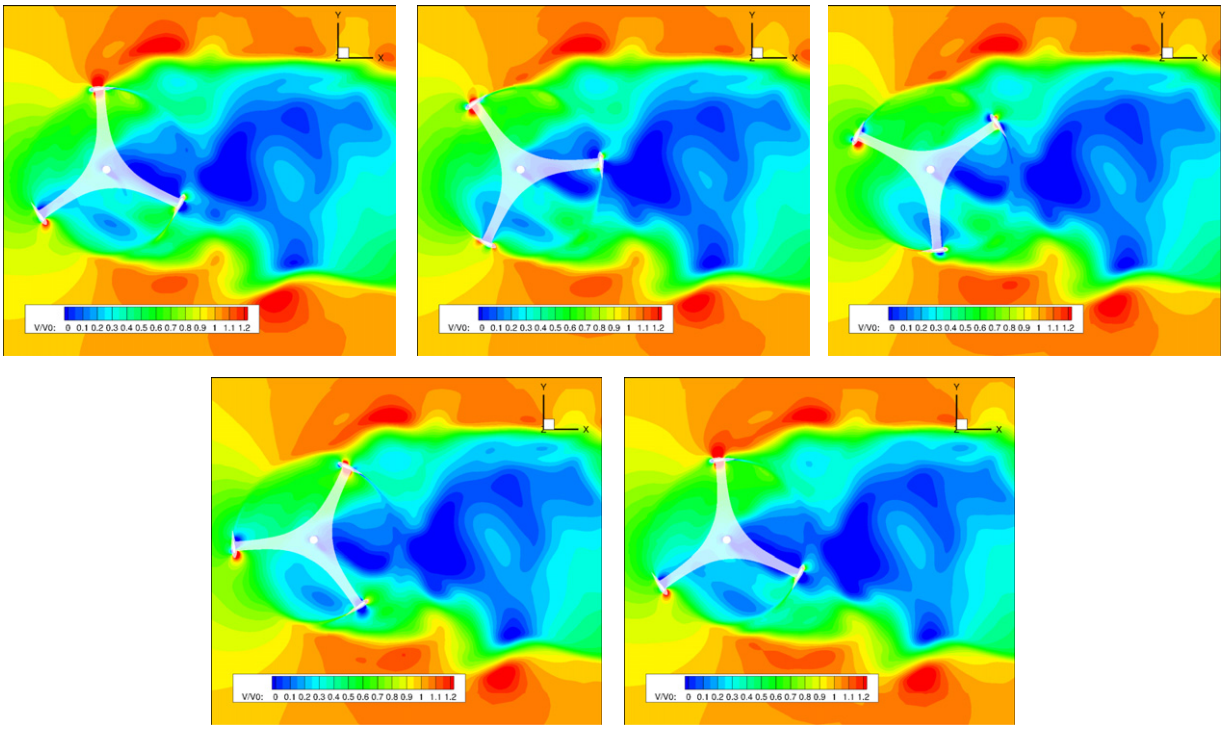

Fig. 4. Velocity field for different azimuthal positions ($\Delta\theta = 30^\circ$) and for $\lambda = 2.5$.

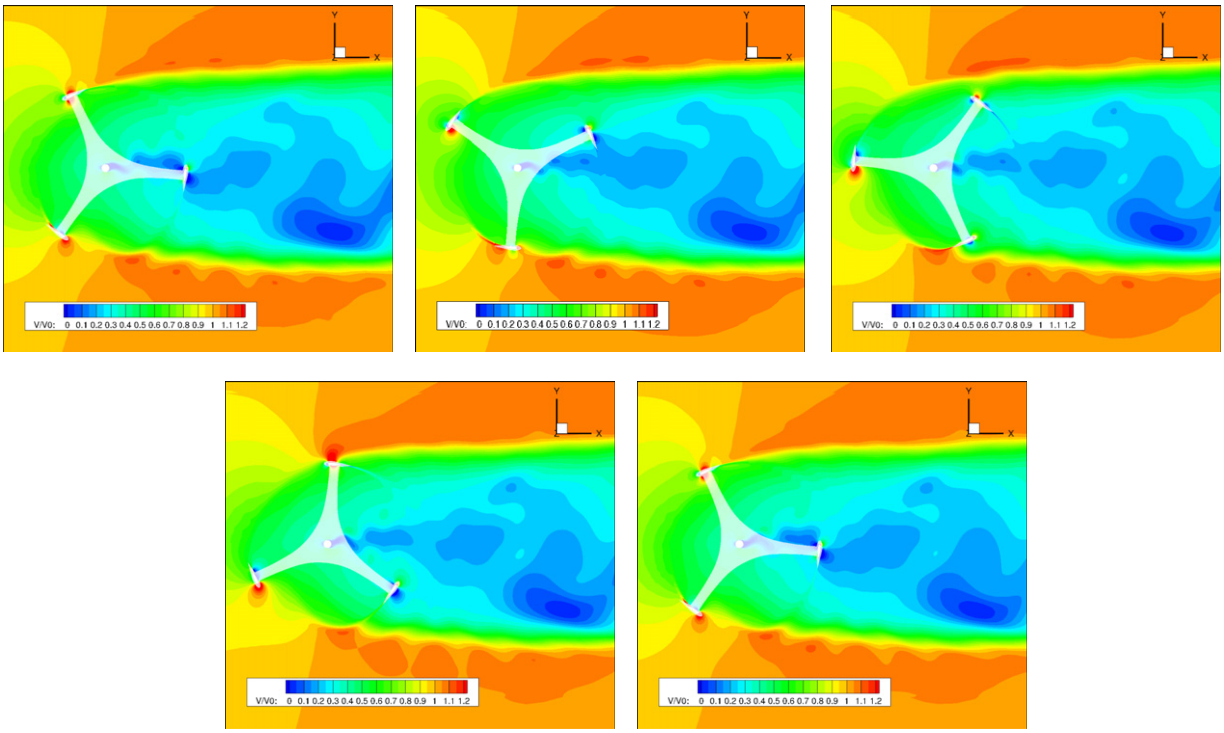

Fig. 5. Velocity field for different azimuthal positions ($\Delta\theta = 30^\circ$) and for $\lambda = 1.52$.

observed also the release of counter-rotating couple of vortices. The latter are not captured by the present RANS simulations, a limit already observed in [6].

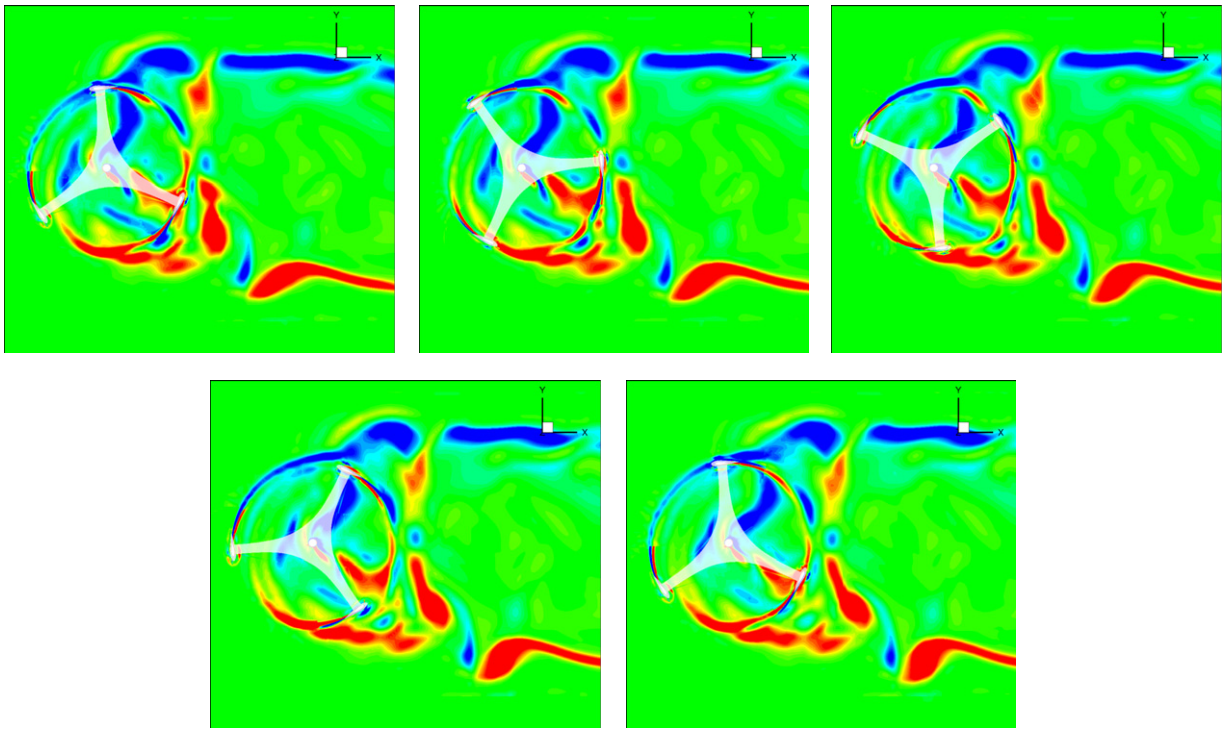

Fig. 6. Z-vorticity for different azimuthal positions ($\Delta\theta = 30^\circ$) for $\lambda = 2.5$.

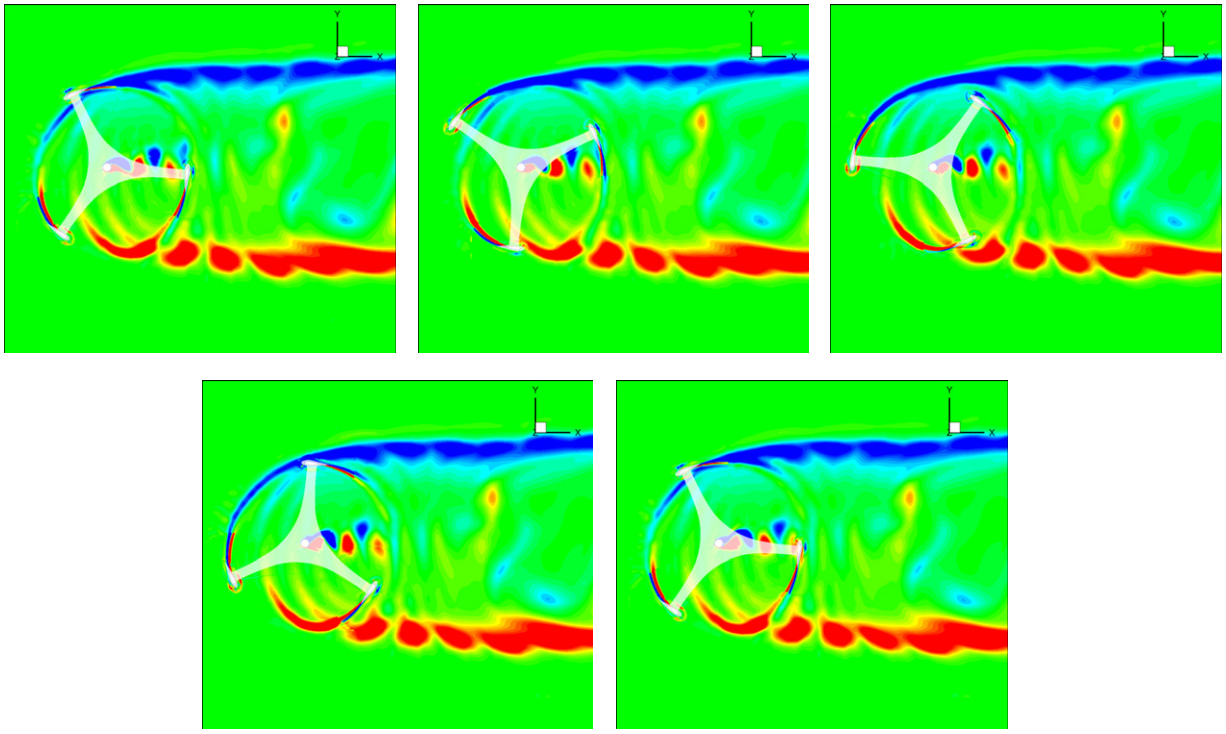

Fig. 7. Z-vorticity for different azimuthal positions ($\Delta\theta = 30^\circ$) for $\lambda = 1.52$.

Also the vorticity field in the symmetry plane (Figs. 6 and 7) is very sensitive to the change of tip speed ratio. At $\lambda = 2.5$, the vorticity field is more irregular and stronger interference effects between the blades and their wakes are observed. The vorticity field at $\lambda = 1.52$ shows clearly the shaft wake and the downstream advection of the wake released by blades

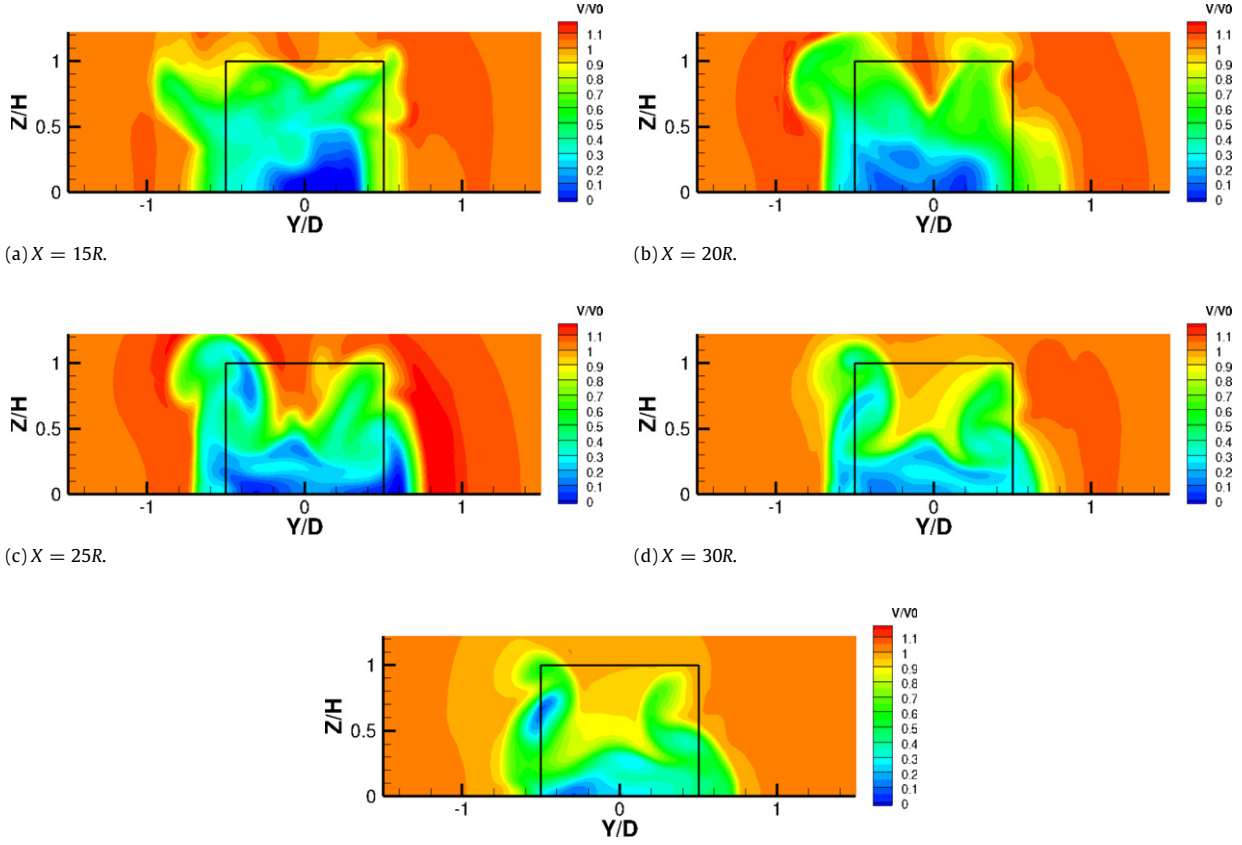

(a) $X = 15R$.

(b) $X = 20R$.

(c) $X = 25R$.

(d) $X = 30R$.

(e) $X = 35R$.

Fig. 8. Velocity module in the Y–Z plane for at distances $X = 15R$, $20R$, $25R$, $30R$, $35R$ for $\lambda = 2.5$.

passing, confirming the results obtained by Howell and collaborators [10]. As expected, both configurations present two lateral large regions of vorticity with opposite sign. These are due to the interaction between the asymptotic wind and the blade passage.

3.2. Normal plane

The velocity field in the normal plane is relevant in understanding the performances of the turbine. Indeed, the power extracted from the flow results in a velocity reduction within the wake. Therefore, a lower velocity is an indication of a higher extracted power. Moreover, flow visualization in the normal plane allows to identify relevant fluid dynamics phenomena, including the tip vortex release.

Five different planes were analyzed, spanning from a $X/R = 1.5$ to $X/R = 3.5$ from the shaft. For $\lambda = 1.52$, see Fig. 9, the velocity module is significantly lower than what observed for $\lambda = 2.5$ (Fig. 8). This suggests that in this configuration wind turbine is potentially more efficient.

For $\lambda = 2.5$, two round-shaped low-speed regions at the two sides of the turbine are observed. These are clearly visible in the $X/R = 3.5$ plane and are possibly related to the tip vortices released by the blades. These vortices are due to the lift generated from the blade. Indeed, the low-speed region is larger in the position corresponding to the advancing blade, i.e. where relative velocity on the blade and hence the lift is larger. As a consequence, vorticity shedding from the blade is larger and tip vortices are stronger. The above can be observed in Fig. 10, where the low-speed regions correspond to high-vorticity regions. Note that the different sign between the left and right regions is coherent to the VAWT rotation.

It is worth noting that tip vortices release is particularly complicated for $\theta = 0^\circ$ and $\theta = 180^\circ$; in these positions the angle of attack changes its sign. Namely, at the top ($\theta = 0^\circ$) the angle of attack switches from positive to negative, whereas at the bottom ($\theta = 180^\circ$) from negative to positive.

Tip vortices release can be observed also in Fig. 11. Fig. 11 shows the Y component of the vorticity in the longitudinal plane ($Y = 0$) before, during and after the passage of a blade: the development of a vortical structure can be clearly seen. In Fig. 11, the vortical structures generated by the support arms are clearly visible.

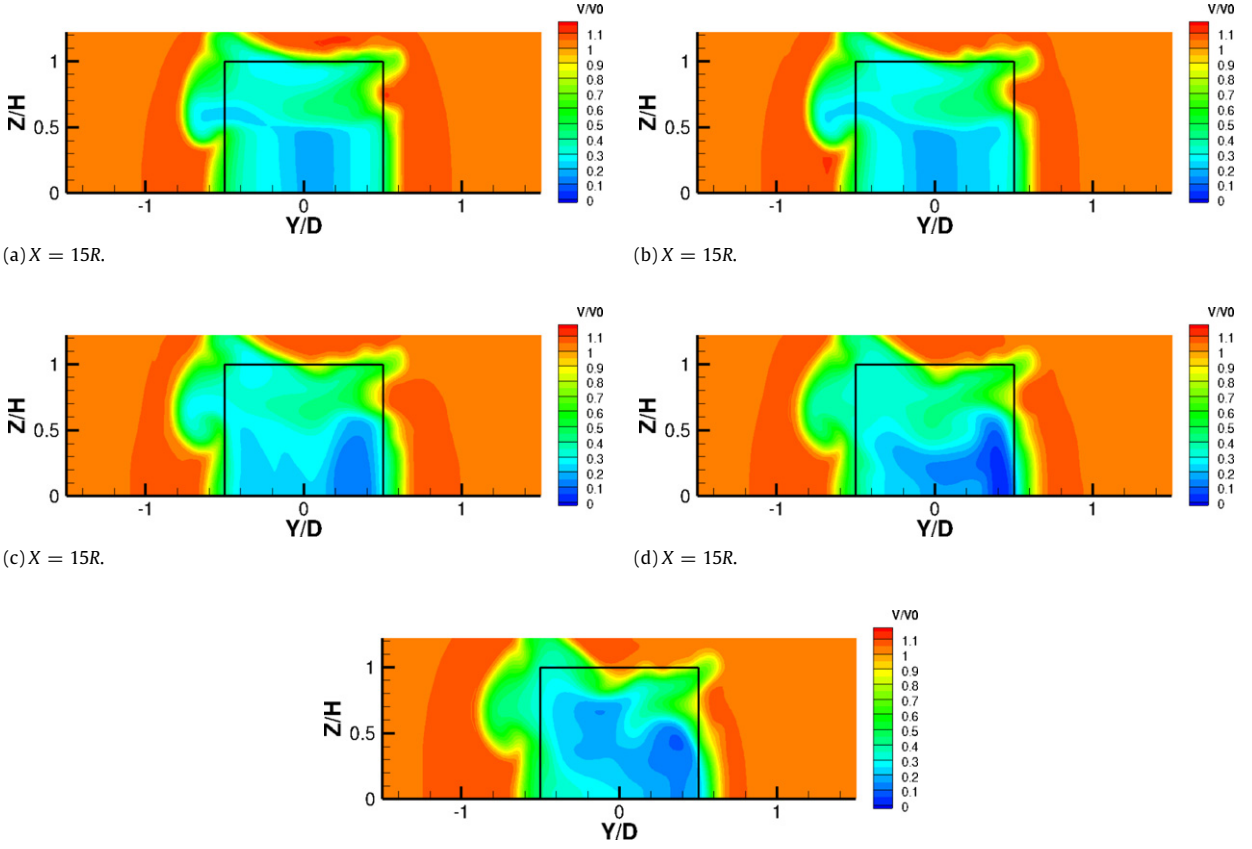

(a) $X = 15R$. (b) $X = 15R$.

(c) $X = 15R$. (d) $X = 15R$.

(e) $X = 15R$.

Fig. 9. Velocity module in the Y–Z plane for at distances $X = 15R$, $20R$, $25R$, $30R$, $35R$ for $\lambda = 1.52$.

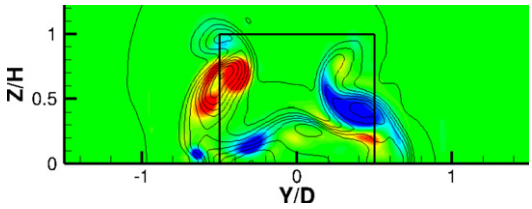

Fig. 10. Velocity and X-vorticity comparison for $X/R = 3.5$ and $\lambda = 2.5$ (X-vorticity flood and velocity lines).

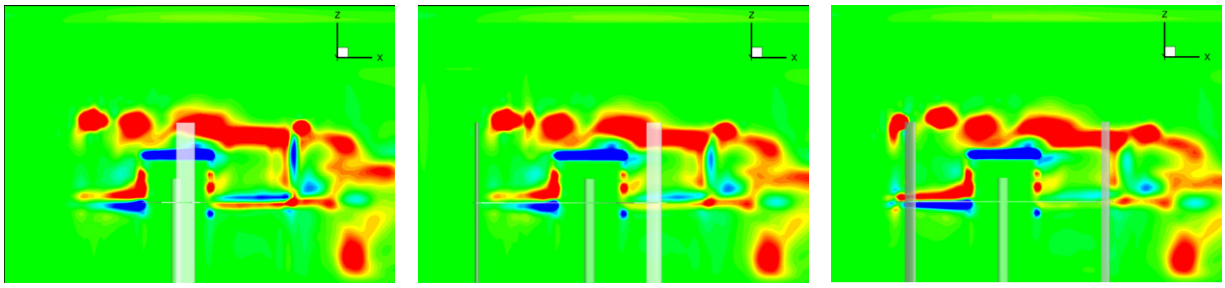

Fig. 11. $Y = 0$ plane—Y-vorticity ($\lambda = 2.5$): before, during and after blade passage.

3.3. Comparison to experimental data

Numerical results were compared to the experimental data obtained by Battisti and collaborators [11]. The comparison shows the phase-averaged velocity field in the normal plane at $X/R = 3$ downstream of the shaft. Phase averaging of the

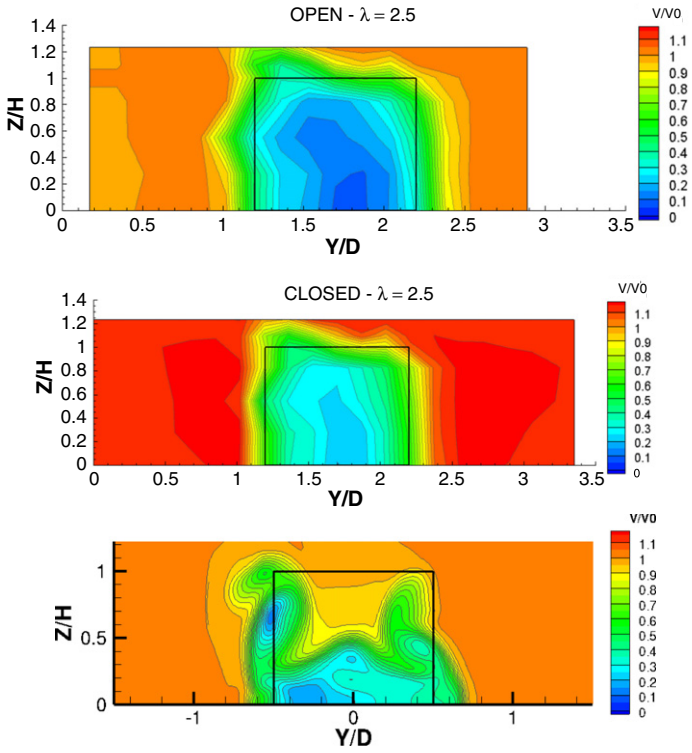

Fig. 12. $X/R = 3.0$ plane—velocity field $\lambda = 2.5$ experimental data for the open (top) and closed (middle) test section – from [11] – and numerical results (bottom).

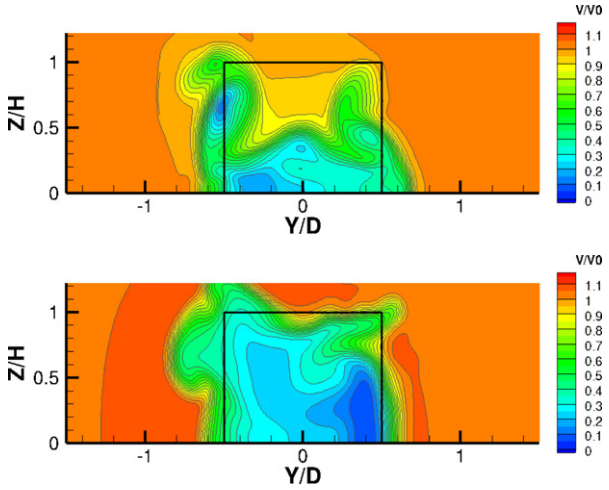

Fig. 13. $X/R = 3.0$ plane, velocity field. Top $\lambda = 2.5$, bottom: $\lambda = 1.52$.

numerical velocity field was obtained by sampling each 10° of rotation. Experimental data are available for the $\lambda = 2.5$ case only.

Significant differences between experimental and numerical results are observed, see Figs. 12 and 13, where numerical simulations are compared to experimental results for the open and closed wind tunnel experimental runs. In particular, in both reference experimental data sets, the flow velocity exhibits an asymmetrical distribution similar to the computed one, although the velocity is lower and more homogeneous.

Even by taking into account the bias due to the relatively small number of measurements points, with 21 points in the Y direction and 9 points in the Z direction, the observed large discrepancy seems to be related to a different functioning regime. In this respect, it is remarkable that, according to measurements, $\lambda = 2.5$ represents the optimal configuration. On the contrary, numerical simulations indicate that the VAWT operates more efficiently at $\lambda = 1.52$ and consistently the optimal

tip speed ratio obtained from simulations is significantly lower then the one obtained from tests. Further investigation, possibly including the wind tunnel walls in the numerical model, are required to confirm these hypothesis.

4. Concluding remarks

Numerical simulations of the flow-field around a three straight blades Vertical Axis Wind Turbine (VAWT) were performed. Two different operating conditions were investigated: $\lambda = 2.5$ and $\lambda = 1.52$. Numerical results, obtained by means of ROSITA software, show relevant aerodynamic features of the flow around vertical axis wind turbine, including the interaction between blades and the complexity of the wake especially in the rotor area. Moreover, for the larger value of the tip speed ratio in the symmetry plane a region of separated flow imputable to dynamic stall was captured. The effect of tip vortices, especially for the $\lambda = 2.5$ configuration, has been highlighted by analyzing the flow-field on the normal planes.

From the velocity field in these planes, some information about performances can be deduced as well: the lower velocity values for $\lambda = 1.52$ suggests that in this configuration the wind turbine extracts more energy from wind. Experimental comparison are not fully satisfactory. At $\lambda = 2.5$ the wake is more regular and presents lower velocity values. These data are more similar to the simulation performed for $\lambda = 1.52$: this apparently surprising result possibly indicates that there is a mismatch between the optimal configuration suggested by tests ($\lambda \sim 2.5$) and the one achievable from simulations.

Further and more accurate analyses and testing should be performed in order to understand reasons of these differences and to achieve, as far as possible, a complete understanding of aerodynamic behavior of the vertical axis wind turbine. According to Ref. [16], in which Detached Eddy Simulation has been employed to simulate a Savonius-type VAWT, a possible improvement can be represented by using a hybrid RANS–LES (Large Eddy Simulation) approach [17], in order to obtain a better description of eddies and vortical structures.

Acknowledgment

The authors would like to thank Dr. Massimo Biava for his support in the use of the ROSITA solver.

References

[1] I. Paraschivoiu, Wind Turbine Design - With Emphasis on Darrieus Concept, first edition, Presses Internationales Polytechnique, 2002.
[2] O. Eboibi, L.A. Danao, R. Howell, J.M. Edwards, A numerical study of the influence of blade profile and solidity on the performance of vertical axis wind turbines, in: AIAA Paper 2013-1095, 2013.
[3] T.J. Carrigan, B.H. Dennis, Z.X. Han, B.P. Wang, Aerodynamic Shape Optimization of a Vertical-Axis Wind Turbine Using Differential Evolution, ISRN Renew. Energy (2012).
[4] L.A. Danao, N. Qin, R. Howell, A numerical study of blade thickness and camber effects on vertical axis wind turbines, Proc. Inst. Mech. Eng. A 226 (2012) 867–881.
[5] C.J. Simão Ferreira, G. van Bussel, G. van Kuik, Wind tunnel hotwire measurements, flow visualization and thrust measurement of a VAWT in skew, J. Sol. Energy Eng. 128 (4) (2006) 487–497.
[6] C.J. Simão Ferreira, H. Bijl, G. van Bussel, G. van Kuik, Simulating dynamic stall in a 2D VAWT: modeling strategy, verification and validation with Particle Image Velocimetry data, J. Phys. Conf. Ser. 75 (2007) Paper number 012023.
[7] N. Fujisawa, S. Shibuya, Observations of dynamic stall on Darrieus wind turbine blades, J. Wind Eng. Ind. Aerodyn. 89 (2001) 201–214.
[8] J.C. Vassberg, A.K. Gopinath, A. Jameson, Revisiting the vertical-axis wind-turbine design using advanced computational fluid dynamics, in: AIAA Paper 2005-47, 2005.
[9] K. Hamada, T. Smith, N. Durrani, N. Qin, R. Howell, Unsteady flow simulation and dynamic stall around vertical axis wind turbine blades, in: AIAA Paper 2008-1319, 2008.
[10] R. Howell, N. Qin, J. Edwards, N. Durrani, Wind tunnel and numerical study of a small vertical axis wind turbine, Renew. Energy 35 (2010) 412–422.
[11] L. Battisti, L. Zanne, S. Dell'Anna, V. Dossena, G. Persico, B. Paradiso, Aerodynamic measurements on a vertical axis wind turbine in a large scale wind tunnel, J. Energy Resour. Technol. 133 (2011).
[12] P.R. Spalart, S.R. Allmaras, A one-equation turbulence model for aerodynamic flows, in: AIAA Paper 92-0439, 1992.
[13] G. Chesshire, W.D. Henshaw, Composite overlapping meshes for the solution of partial differential equations, J. Comput. Phys. 90 (1990) 1–64.
[14] M. Biava, RANS computations of rotor/fuselage unsteady interaction-al aerodynamics, Doctor of Philosophy Thesis, Politecnico di Milano, Milano, Italia, 2007.
[15] J.C.R. Hunt, A. Wray, P. Moin, Eddies, Stream, and Convergence Zones in Turbulent Flows, Center for Turbulence Research Report CTR-S88, 1988.
[16] I. Dobrev, F. Massouh, CFD and PIV investigation of unsteady flow through Savonius wind turbine, Energy Procedia 6 (2011) 711–720.
[17] J. Fröhlich, D. von Terzi, Hybrid LES/RANS methods fort the simulation of turbulent flows, Prog. Aerosp. Sci. 44 (5) (2008) 349–377.